Temperature profile dynamics in QSH regimes with multichords Soft X-Rays diagnostic in RFX-mod

A. Ruzzon, A. Fassina, P. Franz, M. Gobbin, L. Marrelli

Consorzio RFX – Associazione Euratom-ENEA – Padova, Italy

Reversed Field Pinch (RFP) plasmas can spontaneously access improved confinement regimes (Quasi Single Helicity states, QSH [1]) in which one single mode dominates the magnetic perturbation spectrum (with periodicity *m=1, n=-7* in RFX-mod) and a magnetic island with the same helicity appears [2]. For large amplitudes of the dominant mode the island separatrix is expelled and the magnetic topology is characterized by a single helical magnetic axis. These states are labeled SHAx (Single Helical Axis) and are characterized by a helically symmetric core plasma surrounded by electron internal transport barriers (ITBs) [3]. This work is dedicated to analyze the electron temperature profile dynamic and its statistical properties in several QSH plasmas. To this end a database including 157 shots, for a total of more than 500 QSH intervals, has been created. The temperature profiles are obtained by the two foil technique, thanks to high time resolution Soft X-Rays (SXR) diagnostic (up to 10kHz) viewing along 19 lines of sight as shown in Fig. 1a. To take into account the non-axisymmetric geometry of QSH plasmas, a radial coordinate is introduced, ρ, proportional to the normalized magnetic flux enclosed by the helical flux surfaces. The T_e measured along a line of sight is associated to the minimum ρ along the same line, i.e. to the ρ corresponding to the helical surface tangential to the line of sight [4]. By this procedure, a $T_e(\rho)$ profile is obtained.

As the flux coordinate rho also includes the magnetic topology evolving in time, it is not straightforward to compare $T_e(\rho)$ profiles, and in particular their gradients, at different times.

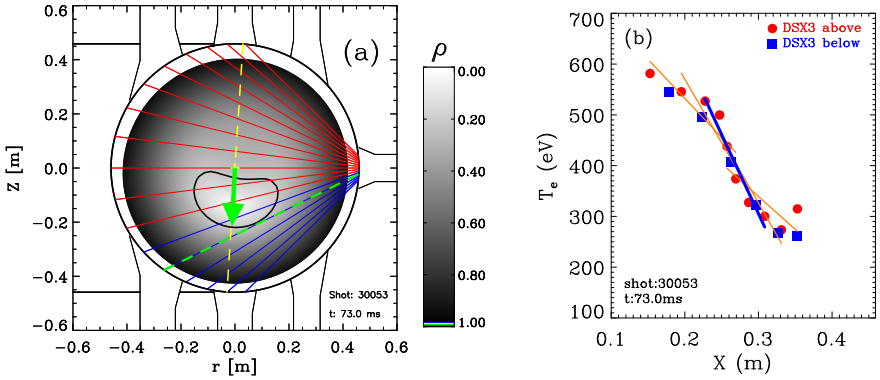

Fig. 1. (a) In grayscale, a typical contour plot of the radial helical coordinate ρ during a SHAx state and, with the green arrow, the X coordinate definition related to the dashed green line of sight: it is the distance from the center of the vessel to the external side of the helical flux surface, the black curve, tangential to the line of sight. Here the red chords represent the lines of sight above the helical axis while the blue ones pass below it. (b) Example of temperature gradient determination. The ∇T_e is the steepest slope (blue thick line) among the linear fits performed on the entire $T_e(X)$ profile (orange thin lines).

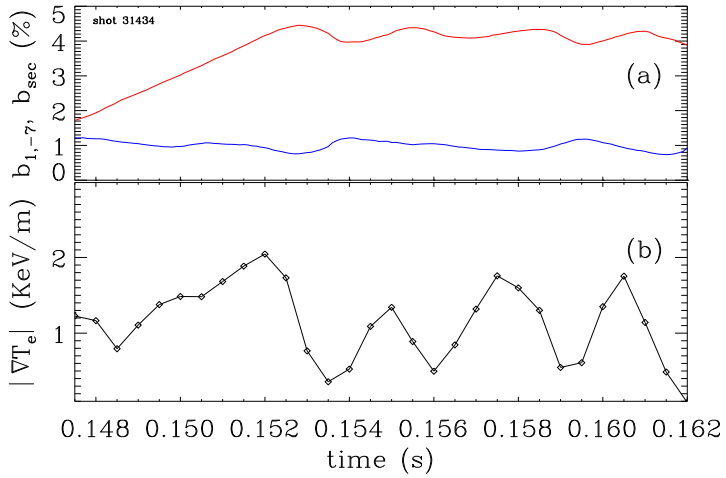

Fig. 2. The ∇T_e evolution for shot 31434 between 147.5 and 162 ms: (a) The red line represents the dominant normalized toroidal mode amplitude and the blue line represents the secondary normalized toroidal mode amplitude. (b) The graphics shows the ∇T_e estimation.

Comparisons are then performed by considering $T_e(X(\rho))$ profiles where the $X(\rho)$ coordinate is the distance between the centre of the camera and the outer side of the flux surface labeled by rho, along the straight line connecting the camera centre with the island O-point, as shown in Fig. 1a. Fig. 1b shows the T_e profile as a function of X: the red dots represent the lines of sight above the helical axis shown in Fig 1a while the blue squares are those below.

The electron temperature gradient has been evaluated by performing several linear fits, on 6 adjacent data points, from the center to the edge of the $T_e(X)$ profile. Since small computation errors of ρ might involve misalignments between the temperatures on the two sides of the helical structures (red dots and blue squares in Fig. 1b), only the T_e data belonging to the side of the helical structure with most of the measurements are considered for the gradient computation. The fit relative to the steepest slope of the $T_e(X)$ profile gives the maximum gradient value, labelled hereafter by ∇T_e, while its X position is labelled $X_{\nabla Te}$. For instance, for the T_e profile reported in Fig. 1b the linear fits are shown in orange and the blue thick line corresponds to the steepest one. It is worth to note that the gradient foot position $X_{\nabla Te}$ is well defined for sharp gradients, as for a flat profile the linear fits are very similar and an univocal choice for $X_{\nabla Te}$ is difficult.

Fig. 2 reports an example of QSH cycle. It can be divided in two time intervals: a *rising* phase (148-153ms), where the dominant magnetic mode grows, and a *flattop* phase, where the dominant magnetic mode keeps its value, with some slight oscillations, till the end of the cycle. This subdivision has been chosen because a different ∇T_e behavior has been recognized during the two phases, as explained in the

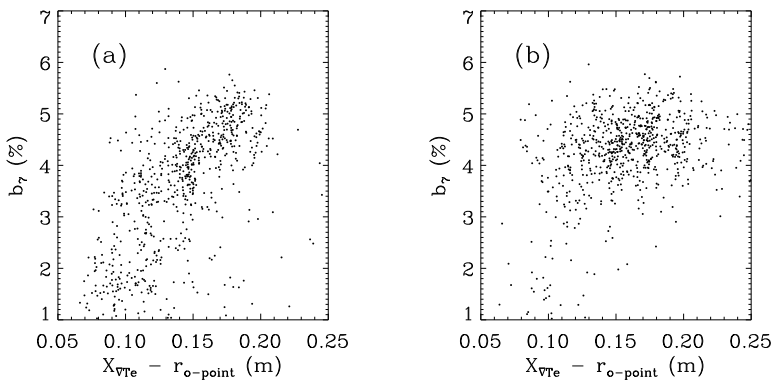

Fig. 3. The dominant magnetic mode, normalized to the edge magnetic field, plotted against the difference between X and $r_{o\text{-}point}$. The *rising* phase is in (a), the *flattop* phase is in (b).

following. ∇T_e values are computed every 0.5ms.

For statistical analysis the gradients lower than $0.1\cdot(\nabla T_e^{max} - \nabla T_e^{min}) + \nabla T_e^{min}$ (10th percentile) and above $0.9\cdot(\nabla T_e^{max} - \nabla T_e^{min}) + \nabla T_e^{min}$, (90th percentile) have been considered, where ∇T_e^{min} and ∇T_e^{max} are respectively the minimum and maximum gradient values of each phase. With this choice all the phases, even if short, are represented by at least one value of ∇T_e. Fig. 3 shows the dominant magnetic mode amplitude plotted against the size of the helical structure, given by the difference between $X_{\nabla Te}$ and the o-point radius ($r_{o\text{-}point}$), for the gradients above the 90th percentile; the plots relative to the *rising* and the *flattop* phase are reported in (a) and (b) respectively. The choice to consider only the highest ∇T_e values is due to the fact that, as explained above, the estimate of $X_{\nabla Te}$ can fail when the T_e profile is flat or has a low gradient. A growing trend can be observed in panel (a) relative to the rising QSH phase: the higher the dominant magnetic mode, the larger is the helical structure. This experimental result is in agreement with similar findings obtained from previous numerical simulations [5]. The same behavior does not hold during the *flattop*: here the helical structure dimension spreads from 10 to 20 cm although the dominant magnetic mode amplitude has a constant value.

Other differences can be noted from Fig. 4(a) and (b): the *rising* phases are characterized by higher gradient values than during the *flattops*. In the *rising* phase, the gradients show a tendency to grow as secondary modes decrease; during the *flattop* this trend is visible only for the gradients above the 90th percentile.

In order to distinguish the cases with steep temperature profile from others with low gradients or flat, the distribution for the flattop phase of the $\nabla T_e/T_e^{core}$ values above the 90th percentile and below the 10th percentile is reported in Fig. 4c, in red and blue respectively (T_e^{core} is the electron temperature on the helical axis). Comparing these distributions $\nabla T_e/T_e^{core} \sim 2\text{m}^{-1}$ has been identified as the value which separates them, therefore such threshold can be used to distinguish the cases with or without a helical thermal structure. In order to investigate the time duration of high gradient helical structures, the intervals when $\nabla T_e/T_e^{core} > 2\text{m}^{-1}$ have

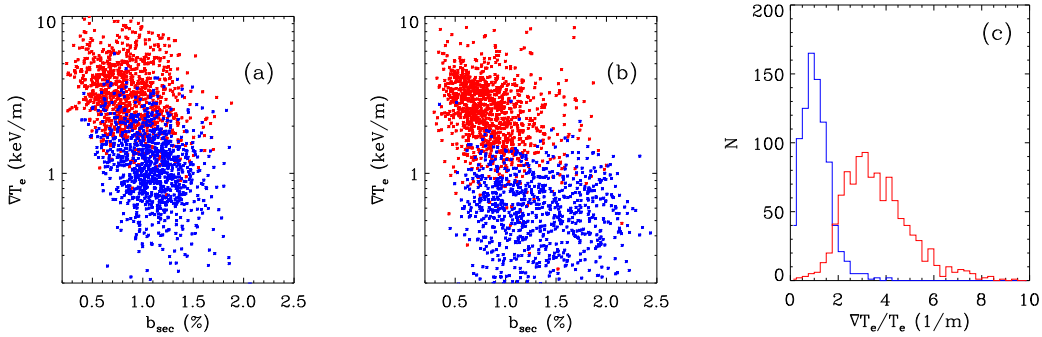

Fig. 4. (a) and (b) The ∇T_e values against the secondary modes normalized to the edge magnetic field. The gradients above the 90th percentile are shown in red and those below the 10th in blue. (a) is referred to the *rising* phases and (b) to the *flattop*. (c) The $\nabla T_e/T_e^{core}$ distribution for the *flattop*: the blue curve is for the gradient values below the 10th percentile and the red curve is for those above the 90th percentile.

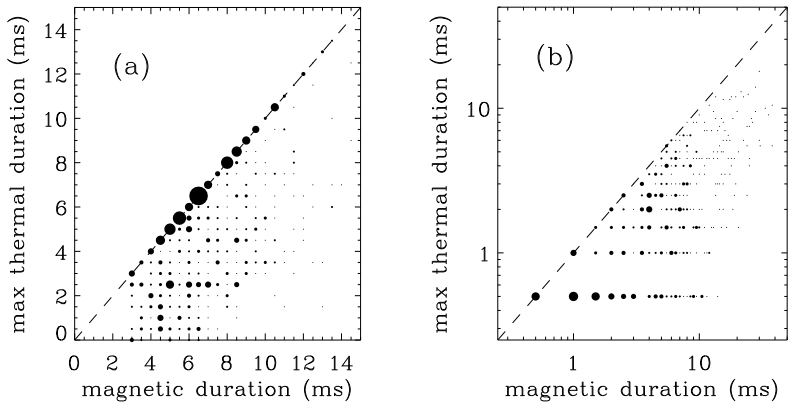

Fig. 5. (a) The Maximum Thermal Duration (MTD), defined as the length of longest interval with $\nabla T_e/T_e$ values higher than $2m^{-1}$, plotted against the respective *rising* phase length (Magnetic Duration). (b) The MTD plotted against the *flattop* length. Here the logarithmic scale has been used since a wider range of intervals is present.

been selected for each *rising* or *flattop* phase. The results for the entire database are reported in Fig. 5, where the abscissas represent the "magnetic duration" (MD), i.e. the *rising* or *flattop* duration, and the ordinates correspond to the "maximum thermal duration" (MTD), i.e. the length of the longest interval with $\nabla T_e/T_e^{core}$ above the threshold of $2m^{-1}$. The dot dimensions are proportional to the number of QSH cycles with the same values of (MD, MTD). Panel (a) is referred to the *rising* phase: most of the cases lay on the dashed line corresponding to MD=MTD or very close to it; this means that $\nabla T_e/T_e^{core}$ is almost always above the threshold during the *rising* phase and. Panel (b) shows the *flattop* phase: helical states longer than 10 ms are rare and fewer cases have the same thermal and magnetic duration. This means that during the *flattop*, transitions to non-helical states may occur with a significant frequency.

In conclusion, this work reports the first analyses concerning electron temperature in QSH states investigated with a high time resolution SXR diagnostic in RFX-mod. The temperature gradient evolution statistically shows a different dynamic in phases where the dominant mode is rising or when saturates to a quasi-constant high amplitude. In particular, in this latter phase back transitions to flat or low gradient profiles occur in most of the analyzed QSH cycle. The reason for this behaviour is still under investigation and may be correlated not only with the secondary modes dynamic but also to other kind of instabilities.

[1] Puiatti M. E. et al., Nucl. Fusion 51, 073038 (2011)
[2] Martin P. et al., Phys. Control. Fusion 49, A177 (2007)
[3] Lorenzini R. et al., Phys. Rev. Lett. 101, 025005 (2008)
[4] Ruzzon A. et al., Proceedings 38th EPS Conference on Plasma Physics, Strasburg, 27/6-1/7 2011, P4.058
[5] Gobbin M. et al., Phys. Rev. Lett. 106, 025001 (2011)